GPS scintillation enhancements associated with aurora and cosmic radio noise absorption

P H Stoker[1], P J Cilliers[2], B D L Opperman[2], C Steyn[1], R V Meyer[2]
[1] Unit for Space Physics, North-West University, Potchefstroom 2520, South Africa
[2] Hermanus Magnetic Observatory, P.O. Box 32, Hermanus 7200, South Africa

[1] **Abstract:** The coincidence of ionospheric scintillation at L-band frequencies with auroral arcs and increased riometric absorption was observed from 01:00 UT on 28 April 2007 by co-located instruments at 72ºS in Antarctica during the recovery phase of a substorm. At about 01:31 UT a stable omega-like arc structure formed with pulsating patches equator ward and dark regions east of the pole ward direction. This structure moved fast eastward, slowed down and broke up in pulsating patches. Enhanced ionization associated with this structure and other auroral arcs, as recorded by an all-sky video camera and an 64 beam imaging riometer, was observed to coincide with phase scintillation along ray paths of GPS satellites. Connection between enhanced ionization in the D-region, as implied by enhanced imaging riometric absorption observed in this study, and phase scintillation at GPS frequencies, may be indicative of the height distribution of ionization structures giving rise to scintillations.

1. Introduction

[2] It is well-known that a radio wave propagating through drifting ionospheric small-scale electron density irregularities may experience fluctuations in both its amplitude and phase. The fluctuation characteristics depend on the transmission frequency and fluctuations in electron density [*Forte*, 2005].

[3] Well-defined regions (patches) of enhanced polar cap *F*-region plasma density have been observed, beginning with the Chatanika incoherent radar scatter measurements [*Banks et al.,* 1974, for reviews eg. *Pedersen et al.,*1998]. The production period of scintillation events in the *F*- region was found to be 5-10 min and the decay time 10-20 min [*Sojka and Schunk,* 1986].

[4] At high latitudes the dynamics of the nighttime auroral ionosphere is partly determined by the dynamics of electron precipitation causing ionization. The lower precipitating energies produce ionization in the *F*-region while the *E*-region is ionized by the higher energies. Both these regions may contribute to changes in the total electron content (TEC) and to TEC perturbations and scintillations. *Kintner et al.* [2002] observed short timescales of one to a few minutes in TEC events, which ruled out the *F*-region ionosphere as a source of their TEC variations. After analyzing their observations they concluded that the most likely explanation for the two events they observed was *E*-region enhancement of electron density produced by discrete aurora electron precipitation below 150 km. This confirms the results of *Basu et al.* (1993), who presented two case studies of auroral *E*-region plasma structures. *Smith et al*. 2008 observed a scintillation event of 10 second duration associated with an auroral arc in Northern Scandinavia, which they attributed to auroral precipitation in the *E*-region.

[5] Ionospheric scintillation in this paper refers to the rapid temporal fluctuations in the amplitude and phase of trans-ionospheric radio signals at the L-band frequencies (1.57 GHz) of the GPS system. Ionospheric phase scintillations were observed on 28 April (day 118) 2007 at the South African Antarctic research station SANAE-IV (71.67^0S, -2.84^0W, L=4.55, corrected magnetic co-ordinates 62.04 ºS, 47.09ºE). The magnetic activity started on 27 April after a Storm Sudden Commencement (SSC) at about 21:59:23 UT (see Figure 1). Aurora of brightness 4 appeared at about 01:00 UT, 28 April, accompanied by GPS phase scintillation and cosmic radio noise absorption (CRNA). In this study the GPS scintillations are related to all-sky low level white light video camera (ASC) luminosities and enhanced CRNA.

2. Instrumentation and method

[6] Variations in CRNA are obtained in 64 directions at SANAE-IV from the recordings of a 38.2 MHz 64 beam imaging riometer at a sampling rate of 1 Hz. The luminosity of auroral events is recorded by an all-sky video camera at the same location. One second digitized all-sky low level white light video images are mapped onto the angular directions of the 64 RF beams of the imaging riometer in order to interrelate spatial structures and temporal variations of optical aurora emissions and CRNA [*Wilson and Stoker, 2002*].

[7] Ionospheric scintillation is monitored at SANAE-IV by the Novatel GSV4004B GPS Ionospheric Scintillation and TEC Monitor (GISTM), which was installed during the austral summer of 2006-2007. This dual-frequency receiver is specifically configured to measure amplitude and phase scintillation from the L1 frequency GPS signals and ionospheric TEC from the L1 and L2 frequency GPS signals by tracking simultaneously up to 11 GPS satellites. Amplitude and phase scintillations, recorded at 50 Hz and the rms averaged over 60 second intervals, are used in this paper to investigate interrelationships with auroral activity and riometric absorption in the high latitude ionosphere of SANAE-IV on 28 April 2007. Only scintillation data from elevations above 20^0 were selected to minimise the influence of multipath.

[8] Figures 2 and 3 show the -3dB contours of the directional RF power response of the 64 imaging riometer beams, plotted from a function of zenith and azimuth angles. The antenna array is aligned geographically north-south. The beam directions are numbered from the north-west corner, proceeding along the upper (northern) row and the following rows. Limitations to the mathematical model did not allow construction of the four corner beams. Also plotted on Figure 2 are the trails of ray paths from GPS-satellites crossing the beam directions on 28 April 2007 from 00:00 through to 23:59 UT. Figure 3 shows the trails of satellites from 01:00 to 02:00 UT for the period when bright aurora was recorded, with dot sizes proportional to the intensity of the phase scintillations.

[9] Figure 2 depicts the 24 hour GPS-satellite trails of 28 April, 2007 for elevations above 20^0. Only northern, western and eastern outer beams of the imaging riometer are in directions that are crossed by GPS-satellites due to the 55˚ inclination of the GPS satellite orbits.

[10] Figure 3 shows that during the interval, 01:00 to 02:00 UT of bright aurora, enhanced phase scintillations were recorded along the ray paths of GPS satellites PRN9, PRN18, PRN19, PRN22 and PRN28 . GPS satellite PRN28 was at the viewing edge of our all-sky and imaging riometer recorders, while moving westward close to 20^0

elevation. The small scintillations recorded along the ray paths from this satellite cannot be correlated in a meaningful way with ASC and imaging riometer observations, and are not considered in this study. No scintillations were seen along the ray path of GPS satellite PRN26, which was within the viewing direction of beam 48 while crossing the dark ionospheric region (see Figure 6).

3. Observations

[11] A sudden storm commencement (SSC) was recorded at 21:59 UT on 27 April 2007 (day 117) by all three components of the fluxgate magnetometer at SANAE-IV (see Figure 1). Magnetic activity increased from the local K-index of 1 during the interval 18:00-21:00 UT to K=4 before midnight and to K=5 after midnight. Note that local time at SANAE-IV lags universal time by about 11 minutes. Figure 4 shows micropulsations in the geomagnetic H-component as recorded at Hermanus (geographic 34° 25' 28" S, 19° 13' 26" E, corrected geomagnetic coordinates 42° 25' S, 83° 02' E) from 18:00 UT on 27 April until 06:00 UT the following day. A Pi2 pulsation started at about 21:49 UT on 27 April 2007.

[12] Aurora of brightness 2 was observed before local midnight, but was too faint in the moonlit upper atmosphere to be photographed by the ASC. Aurora of brightness 4 appeared just before 01:00 UT on day 118 (28 April, 2007), coinciding with a sharp increase in the Z-component of the geomagnetic field (Figure 1). ASC recording started at 01:06:00 UT. Figure 5 displays 60 second averaged phase scintillations along ray paths of the GPS satellites PRN9, PRN18, PRN19, and PRN22 for the period 01:00 – 02:00 UT.

[13] From 01:07:01 – 01:11:00 UT strong phase scintillations were recorded along ray paths of the GPS satellite PRN9 (see Figure 5). This satellite was then located between the -3dB contours of imaging riometer directions #15 and #23 on Figure 3, at the position marked by the large dot on the PRN9 trail. This position is just below the west-east torch-like structure at 01:08:14 UT in Figure 6a. Superimposed on this torch-like structure were moving pulsating patches.

[14] Figures 7 and 8 show the respective correlation of 1 second aurora luminosity and riometric absorption with 60 second averaged GPS satellite PRN9 scintillation. Larger luminosity (Figure 7) and absorption (Figure 8) were recorded in beam direction #15 than in directions of beams #23 and #31, because beam #15 was then directed into the torch-like structure of Figure 6a..This enhanced luminosity and absorption in beam direction #15 correlate with increased phase scintillation along the ray path of satellite PRN9 for the full duration of enhanced scintillation until 01:11:00 UT. In beam direction #23, luminosity increased only during the minute 01:07:01 – 01:08:00 UT, where after luminosity (Figure 7) decreased, absorption (Figure 10) varied concurrently with scintillation for the full duration of enhanced scintillation until 01:11:00 UT. This difference in enhancements in luminosity and absorption suggests an energy-dependent dispersion of precipitating electrons ionizing the *E* and *D*- regions of the ionosphere.

[15] In beam direction #31 neither the luminosity nor absorption showed enhancements during the period plotted in Figures 7 and 8. The values in direction #31 were below those of the directions #15 and #23. Beam #31 was directed towards a region of low

aurora luminosity colored blue in Figure 6a, pole-ward from the west-east orientated auroral arc.

[16] The largest dots on the trails of GPS satellites PRN22, PRN18 and PRN19 in Figure 3 depict their localities at 01:31 UT when these satellites encountered strong phase scintillations (Figure 5). At this instant the GPS ray paths of these three satellites, PRN22, PRN18 and PRN19, were within directions defined by the -3-dB contours of beams #19, #22, and #33, respectively.

[17] Figures 9 and 10 are respective plots of the phase scintillations along the ray paths of satellites PRN22 and PRN18, together with 1 second luminosities and absorptions recorded in beam directions #19 and #22 from 01:28:01 to 01:34:00 UT. Strong phase scintillations appear to coincide with strong enhancements in both luminosities and absorptions in these respective directions. However, only weak scintillation were observed (Figure 11) along the ray path of PRN9 in beam direction #23 in which direction strong enhancements in luminosity and absorption were also recorded during this time interval.

[18] Strong phase scintillations were observed along the ray path of PRN19 from 01:20:01 to 01:23:00 UT, and again from 01:29:01 to 01:31:00 and 01:35:01 to 01:37:00 UT (Figure 3). The 60 second averaged scintillation from this GPS satellite is plotted in Figure 12 from 01:15:01 to 01:49:00 UT together with luminosities observed in imaging riometer beam directions #41 and #33, of which the -3 dB contours have been crossed by the ray path of PRN19 (Figure 3). Also plotted is the luminosity recorded by beam #34, bordering beam #33. The luminosity of beam #34 shows a slight enhancement during the first interval 01:20:01 to 01:23:00 UT, whereas only spiking luminosities were then recorded by beams #33 and #41.

[19] The enhanced scintillations of PRN19 correlate well with the enhancements in luminosity recorded by beams #33 and #41 for the second and third periods 01:29:01 to 01:31:00 and 01:35:01 to 01:37:00 UT, and also for the smaller subsequent enhancements (Figure 12). No absorptions were seen from the imaging riometer recordings in beam directions #33, #34 or #41, during this period of observation.

[20] A sequence of luminous structures are obvious in Figure 6 from 01:08:14 through to 01:35:00 UT. During this period pulsations occurred along torch-like structures. About 01:30:50 (Figure 6b) a stable omega-like arc structure (Akusofu, 1974, Opgenoorth et al., 1983) started to form, with pulsating patches equator ward and dark regions towards the south east of the arc. These dark regions of minimum luminosity are colored dark blue in Figures 6(b) and 6(c)). This omega-type arc structure of 01:30:50 UT moved fast eastward until 01:31:50 UT (Figure 6c), when it began to break up in pulsating patches and to broaden. The eastern edge continued to move eastwards slowly. Figure 6d pictures this structure at 01:35:00 UT. The moon is visible on the western limb in each of these panels of Figure 6.

[21] In Figure 13 is plotted the luminosities recorded in directions #34 to #39, covering the eastward movement of the omega-type arc structure from 01:29:01 through to 01:33:00 UT. These directions are along the fifth west-east row of the imaging riometer beams (see Figure 3). The strong enhancements in luminosity in directions #34 and #35 from about 01:29:40 to 01:30:30 UT in Figure 13 correlate with the ASC pictures. At about 01:30:50 the luminosity in direction #34 increased again, followed by subsequent

strong enhancements of luminosities in directions #35, #36, and #37 as displayed in Figure 13. The maxima of these enhanced luminosities showed displacements from direction #34 through to direction #37 in the time interval between the respective pictures at 01:30:50 and at 01:31:50 in Figure 6. The speed of these eastward displaced maxima amounts to about 2 km/s at an altitude of 110 km.

[22] A small peak in luminosity above the background level was recorded in direction #39 with a maximum at 01:31:37, between those of directions #36 and #37 (Figure 13). No enhancement was seen in direction #38. Similar scenarios are seen in luminosity plots in beam directions along other rows of the imaging riometer directional field.

[23] Absorption recorded by the imaging riometer in beam directions #34 to #39 along the fifth west-east row is displayed in Figure 14. Contrary to the simultaneous peaking in Figure 13 of luminosities during the interval 01:29:40 to 01:30:30 UT, a fairly random peaking in absorption appears in Figure 14. Furthermore, instead of subsequently displaced maxima in directions #34 through to #37, as observed in luminosities from 01:30:50 to 01:31:50 UT (Figure 13), there is a subsequent displacement in up-going slopes of absorption enhancements in directions #34 through to #38 (Figure 14). These temporal differences in auroral luminosity and riometric absorption in subsequent directions imply a time-dependent directional dispersion in the electron precipitating energy spectrum. These differences may be signatures of a reorganization of the magnetospheric magnetic field during the recovery phase of a strong substorm

[24] A strong variation is seen in luminosity plots of beam #15 in Figure 7. This variation should relate to pulsating patches, observed along the west-east orientated arc displayed in Figure 6a. No excessive fluctuation is seen in absorptions in beam direction #15 as displayed in Figure 10. In beam direction #19, Figure 9, there are strong variations in both luminosity and absorption before 01:30:50 UT. Beam #19 was then directed towards the torch-like pulsating structure when the omega-like structure started to form (Figure 6b). It is difficult to say whether the strong variation in absorption was also related to the pulsating patches in the visible aurora because variations in CRNA recordings do appear at times.

4. Discussion and conclusion

[25] It is well-known that large scale wave structures develop along the poleward boundary of the diffuse aurora during the early morning sector in the late recovery phase of a large substorm, resulting in a sequence of dark holes. The brighter aurora band around a dark hole resembles then an inverted Greek capital letter omega [Opgenoorth et al., 1983]. These omega bands drift eastward with a velocity close to the ionospheric **E** x **B** velocity [Opgenoorth et al., 1994, Akasofu, 1974]. Apparently the ASC aurora pictures in Figure 6 may be associated with the development and eastward drift of an omega band, with pulsations equatorward of the band.

[26] Different trends between absorptions and luminosities are apparent in several viewing directions of the imaging riometer when Figures 7 and 8 and Figures 13 and 14 are inter compared. These different trends suggest an energy-dependent dispersion in directions of precipitating electrons ionizing the *E*-region, where aurora luminosity originates, and the *D*-region, where CRNA is maximum. This energy-dependent precipitation may be indicative of a reorganization of the magnetospheric magnetic field during the recovery phase of a strong substorm.

[27] Aurora displays originate from precipitation of electrons which generate optical emissions from the E and F regions. These optical displays are focused on the focal plane of the all-sky camera, on which the -3 dB contours of the 64 beams of the imaging riometer have been projected also, as depicted in Figure 3. Absorption of cosmic radio waves are due to ionization of the E- and D- regions, with a maximum at about 90 km [Hargreaves, 1980]. The projections of the angular -3 dB contours of Figure 3 to an altitude of 115 km for aurora luminosity and 90 km for riometric absorption, show strong outward extensions of the outer beams of the imaging riometer (Figure 15). The spiking luminosities, recorded in beam directions #33 and #41 during the interval 01:20 to 01:23 UT (Figure 12), originated, therefore, from an broad projected area of aurora emissions. Adjacent beam #34 did show only a small enhancement and no spikes in luminosity. Although not convincing, the spiking luminosity may, therefore, be accepted to support this paper's general observation of correlation between phase scintillation and aurora luminosity.

[28] It is well-known that a radio wave, propagating through drifting ionospheric small-scale electron density irregularities, may experience fluctuations in both its amplitude and phase. No significant ionospheric amplitude scintillations at GPS frequencies were observed in this investigation, but several strong phase scintillations were evident, coinciding with either or both *E*- and *D*-region enhanced ionization as signified, respectively, by aurora luminosity and cosmic radio noise absorption. The lack of significant amplitude scintillation, as expressed by the S4-index, may be due to the shorter ray paths through the ionosphere of GPS satellites of this study of which the elevation angles were between ~30º and 25^0 (PRN19), and larger. The ionospheric small-scale electron density irregularities caused by electron precipitation in the *E*- and *D*-regions enhanced phase scintillation, but was presumably not large enough for amplitude scintillations to occur along the ray paths of GPS satellites with elevation angles above ~25^0.

[29] The energy spectrum of precipitating electrons, that cause aurora, varies from eV to tens of keV. The lower energies produce ionization in the *F*-region, while higher energies ionize *E*- and *D*-regions, This study confirms that riometric absorption correlates in time with aurora luminosity, but it also suggests that *D*-region ionization may contribute to small-scale electron density irregularities producing GPS scintillations together with contributions from the *E*- and *F*-regions.

[30] **Acknowledgements.** HMO and NWU participation in this research was supported by SANAP grants SNA2005081500001 and SNA2007051400001**.** Dr Andrew Collier is thanked for his proposed corrections to the manuscript.

References

Akasofu, S-I.. (1974), A study of auroral displays photographed from the DMSP-2 satellite and from the Alaska meridian chain stations, *Space Science Reviews* 16, 617-725.

Banks, P. M., C. 1. Rino, and V. B. Wickwar (1974), Incoherent scatter radar observations of westward electric fields and plasma densities in the auroral ionosphere,

J. *Geophys. Res.,* 79, 187-198.

Basu, S., E. J. Weber, T. W. Bullet, M. 1. Keskinen, E. MacKenzie, P. Doherty, R. Sheehan, H. Kuenzler, P. Ning, and J. Bongiolatti (1998), Characteristics of plasma structuring in the cusp/cleft region at Svalbard, *Radio Sci., 33,* 1885-1899.

Basu, SU., E. MacKenzie, S. Basu, H. C. Carlson, D. A. Hardy, F. 1. Rich, and R: C. Livingston (1983), Coordinated measurements of low-energy electron precipitation and scintillations TEC in the auroral oval, *Radio Sci., 18,* 1151-1165. .

Basu, Su., S. Basu, R. Eastes, R. E. Huffinan, R. E. Daniell, P. K. Chaturvedi, C. E. Valladares, and R. C. Livingston (1993), Remote sensing of auroral *E* region plasma structures by radio, radar, and UV techniques at solar minimum, *J. Geophys. Res.,* 98, 1589-1602.

Forte, B. (2005), Optimum detrending of raw GPS data for scintillation measurements at auroral latitudes, *Journal of Atmospheric and Solar-Terrestrial Physics* 67, 1100-1109

Hargreaves, J. K. D-region electron densities observed by incoherent-scatter radar during auroral-absorption spike events, *J. Atmos. Terr. Phys*., 42, 783-789, 1980.

Kintner, P.M., H. Kil, C. Deehr, and P. Schuck (2002), Simultaneous total electron content and all-sky camera measurements of an auroral arc, *J. Geophys. Res., 107*, A7, 10.1029/2001JA000110, SIA 13-1 – SIA 13-6.

Opgenoorth, H.J., J. Oksman, K.U. Kaila, E. Nielsen, and W. Baumjohann (1983), Characteristics of eastward drifting omega bands in the morning sector of the oral oval, *J. Geophys. Res.,* 88, 9171-9185.

Opgenoorth, H.J., M.A.L. Persson, T.I. Pulkkinen, and R.J. Pellinen (1994), Recovery phase of magnetospheric substorms and its association with morning-sector aurora, *J. Geophys. Res*. 99, 4115-4129.

Pedersen, T. R., B. G. Fejer, R. A. Doe, and E. J. Weber (1998), Incoherent scatter radar observations of horizontal F-region plasma structure over Sonderstrom, Greenland, during polar cap patch events, *Radio Sci.,* 33(6), 1847-1866.

Smith, A. M., Mitchell, C. N., Watson, R. J., Meggs, R. W., Kintner, P. M., Kauristie, K., Honary, F. (2008), GPS scintillation in the high arctic associated with an auroral arc, *Space Weather*, 6 (3), 1-7, S03D01, doi:10.1029/2007SW000349.

Sojka, J. J., and R. W. Schunk (1986), A theoretical study of the production and decay of localized electron density enhancements in the polar ionosphere, *J. Geophys. Res.,* 91, 3245-3253. .

Wilson, A. and P.H. Stoker, Imaging riometer observations on energetic electron precipitation at Sanae IV, Antarctica (2002), *J. Geophys. Res., 107,* A10, 1268, doi:10.1029/2000JA000463, SMP 2-1 – SMP 2-10.

CAPTIONS TO FIGURES

Figure 1. Geomagnetic H-, D-, and Z-components at SANAE-IV of 27 and 28 April, 2007 (days 117 and 118) from 20:00-08:00 UT

Figure 2. Trails of GPS ray paths of elevation larger than 20^0 recorded at SANAE-IV for the whole day of 28 April, 2007, 00:00-23:59 UT, superimposed on the -3-dB contours of 64 beam directions of the imaging riometer projected on the focal plane of the all-sky video camera. The outer circle is the contour of the 90^0 zenith angle.

Figure 3. Trails of GPS ray paths of elevation larger than 20^0 for 28 April, 2007, from 01:00 to 02:00 UT, superimposed on the -3dB contours of 64 beam directions of the imaging riometer. Boldface numbers at the start of each trail (at 01:00 UT) indicate the PRNs of the GPS satellites. The size of the dots along the trails corresponds to the intensity of the phase scintillation at the particular location with the largest dots corresponding to $\sigma_\varphi = 1$.

Figure 4. Micropulsations in the geomagnetic H-component as recorded at Hermanus (geographic 34° 25' 28" S, 19° 13' 26" E, geomagnetic 42° 25' S, 83° 02' E) from 18:00 UT on 27 April until 06:00 UT the following day.

Figure 5. 60 second averaged phase scintillations along ray paths above 20^0 elevation of GPS satellites observed from SANAE-IV on 28 April, 2007 (day 118) from 01:00 to 02:00 UT. The satellite numbers appear next to each graph. The graphs are vertically offset for clarity. The zero-level baseline for each PRN is shown on the left end of each graph.

Figure 6. All sky auroral luminosity superimposed on -3-dB contours of 64 riometer beam directions on 28 April, 2007 at (a) 01:08:14, (b) 01:30:50, (c) 01:31:50, (d) 01:35:00 UT, respectively. Dark red is high luminosity, dark blue low luminosity. North is upwards, east to the right, south below and west to the left. The feature near the western horizon is the setting moon.

Figure 7. The 60 second averaged scintillations of the GPS satellite PRN9.of 28 April, 2007, from 01:06:01 to 01:18:00 UT, and the 1 second luminosities in arbitrary units in directions of imaging riometer beams #15, #23, and #31.

Figure 8. The same as Figure 7, but for riometric absorptions in directions #15, #23 and #31.

Figure 9. The 60 second averaged scintillations of the GPS satellite PRN22 on 28 April (day 118), 2007, from 01:28:01 to 01:34:00 UT, and the 1 second luminosities in arbitrary units and the riometric absorptions in dB in beam direction #19.

Figure 10. The same as Figure 9, but for GPS satellite PRN18 and direction #22.

Figure 11. The same as Figure 10, but for GPS satellite PRN9 and direction #23.

Figure 12. GPS PRN19 60 second phase scintillation on 28 April (day 118), 2007, from 01:15:01 to 01:49:00 UT, and the 1 second luminosities in arbitrary units of beams #33, #34 and #41.

Figure 13. Aurora luminosities in directions #34 - #39 of the 5th West-East row of the imaging riometer beam grid on 28 April, 2007 from 01:29:01 to 01:32:30 UT

Figure 14. Riometric absorptions in directions #34 - #39 of the 5th West-East row of the imaging riometer beam grid on 28 April, 2007 from 01:29:01 to 01:32:00 UT

Figure 15. The projections of the -3 dB angular contours of Figure 3 to the altitudes of 90 km (riometer absorption altitude) and 115 km (aurora altitude) [Wilson and Stoker, 2002].

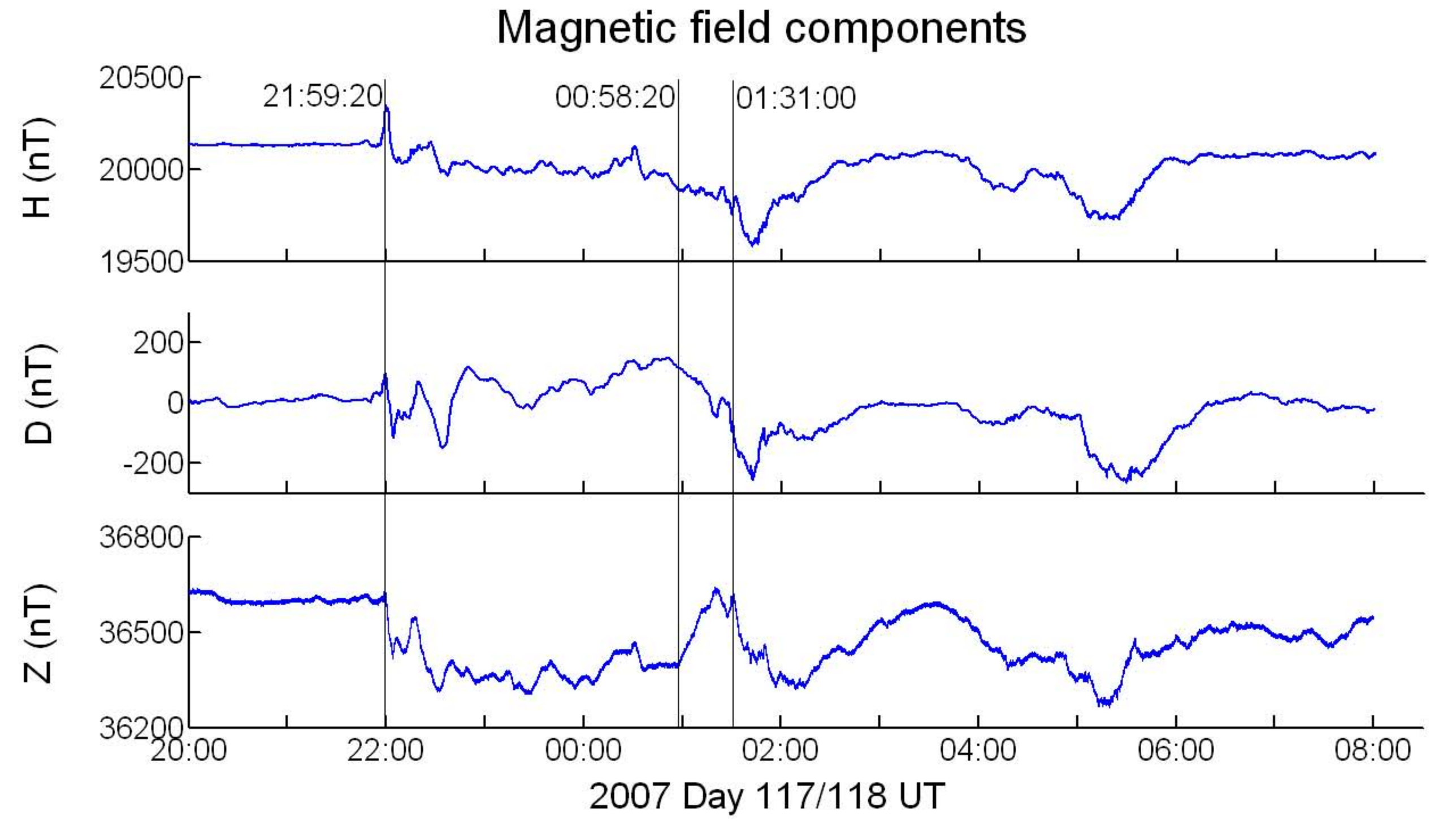
Magnetic field components
H (nT)
D (nT)
Z (nT)
20500
20000
19500
200
0
-200
36800
36500
36200
21:59:20
00:58:20
01:31:00
20:00
22:00
00:00
02:00
04:00
06:00
08:00
2007 Day 117/118 UT

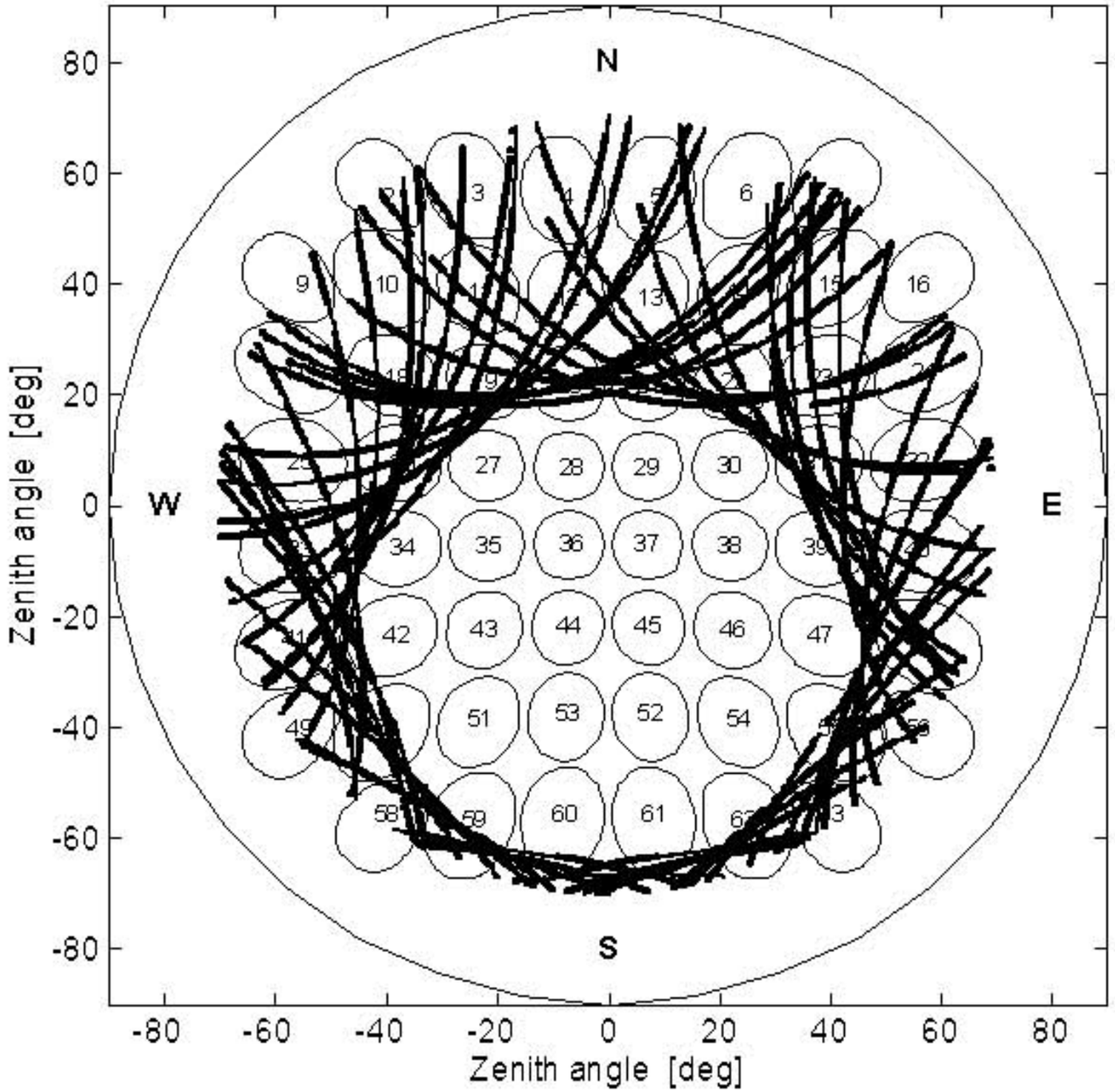
N
S
W
E
Zenith angle [deg]
Zenith angle [deg]
80
60
40
20
0
-20
-40
-60
-80
-80
-60
-40
-20
0
20
40
60
80
3
6
9
10
13
15
16
27
28
29
30
34
35
36
37
38
39
42
43
44
45
46
47
51
53
52
54
58
59
60
61

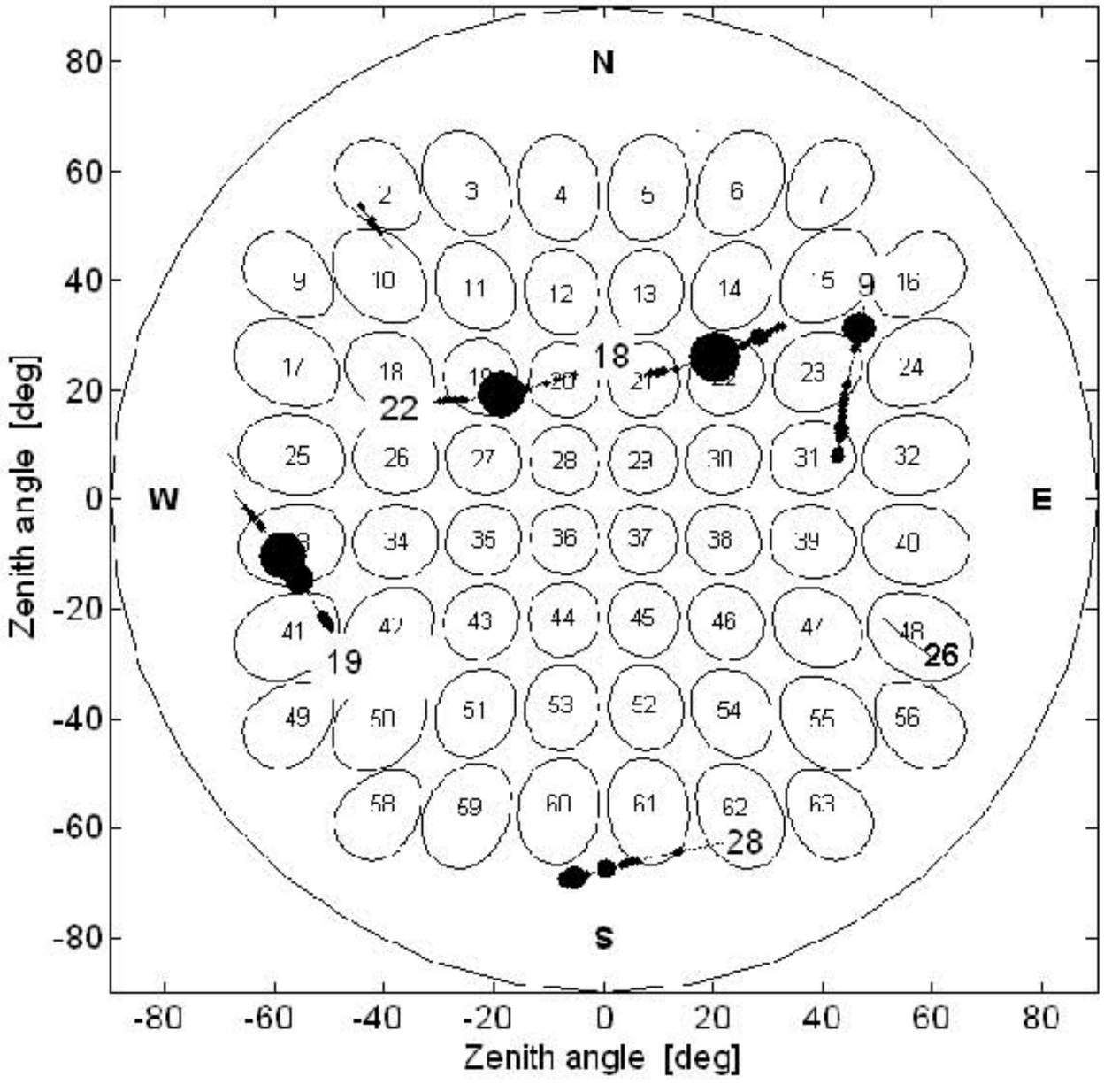
N
W
E
S
Zenith angle [deg]
Zenith angle [deg]
80
60
40
20
0
-20
-40
-60
-80
-80
-60
-40
-20
0
20
40
60
80
2
3
4
5
6
7
9
10
11
12
13
14
15
16
17
18
19
20
21
22
23
24
25
26
27
28
29
30
31
32
33
34
35
36
37
38
39
40
41
42
43
44
45
46
47
48
49
50
51
53
52
54
55
56
58
59
60
61
62
63
9
18
22
19
26
28

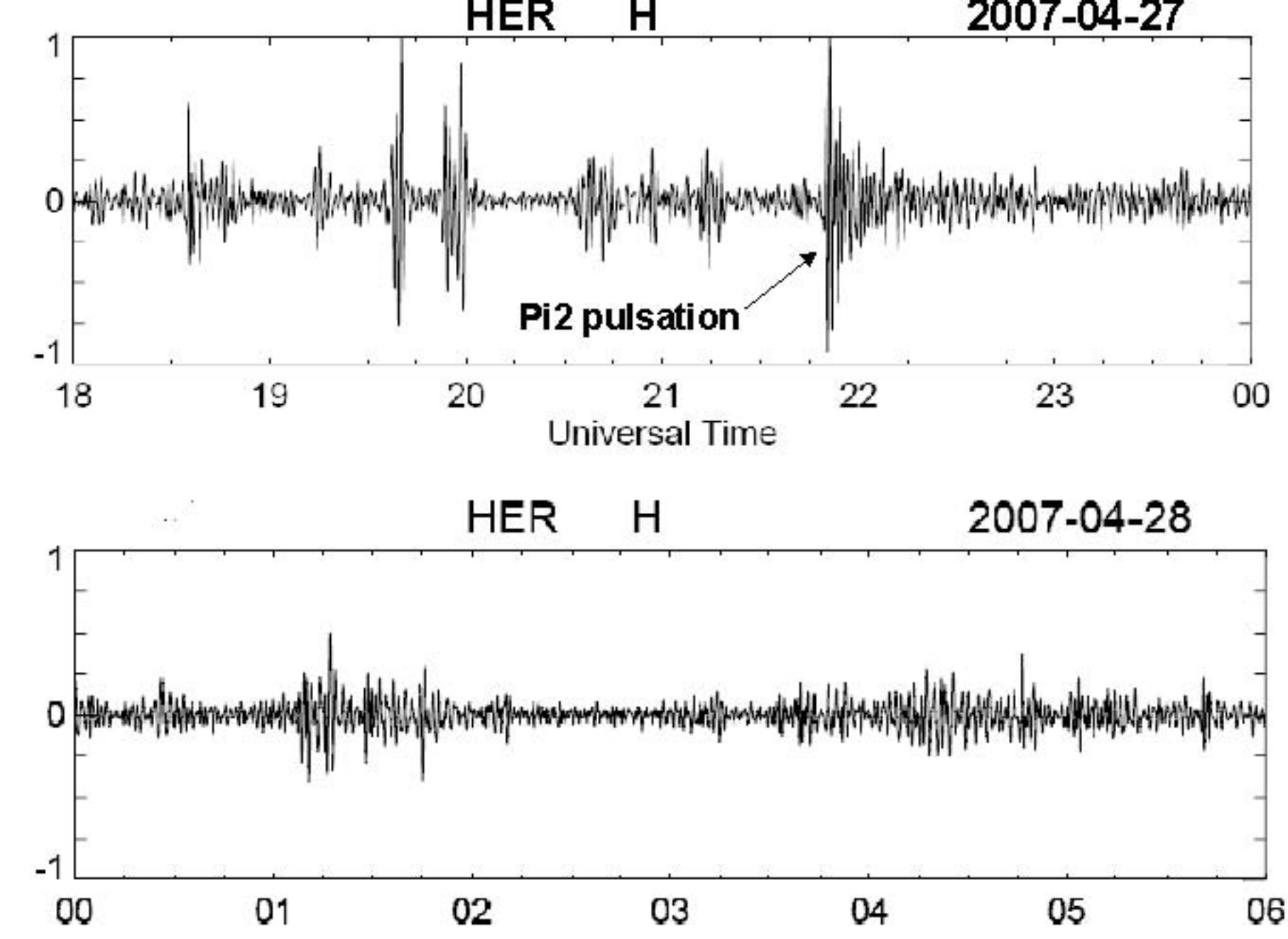
HER H
2007-04-27
1
0
-1
Pi2 pulsation
18
19
20
21
22
23
00
Universal Time

HER H
2007-04-28
1
0
-1
00
01
02
03
04
05
06

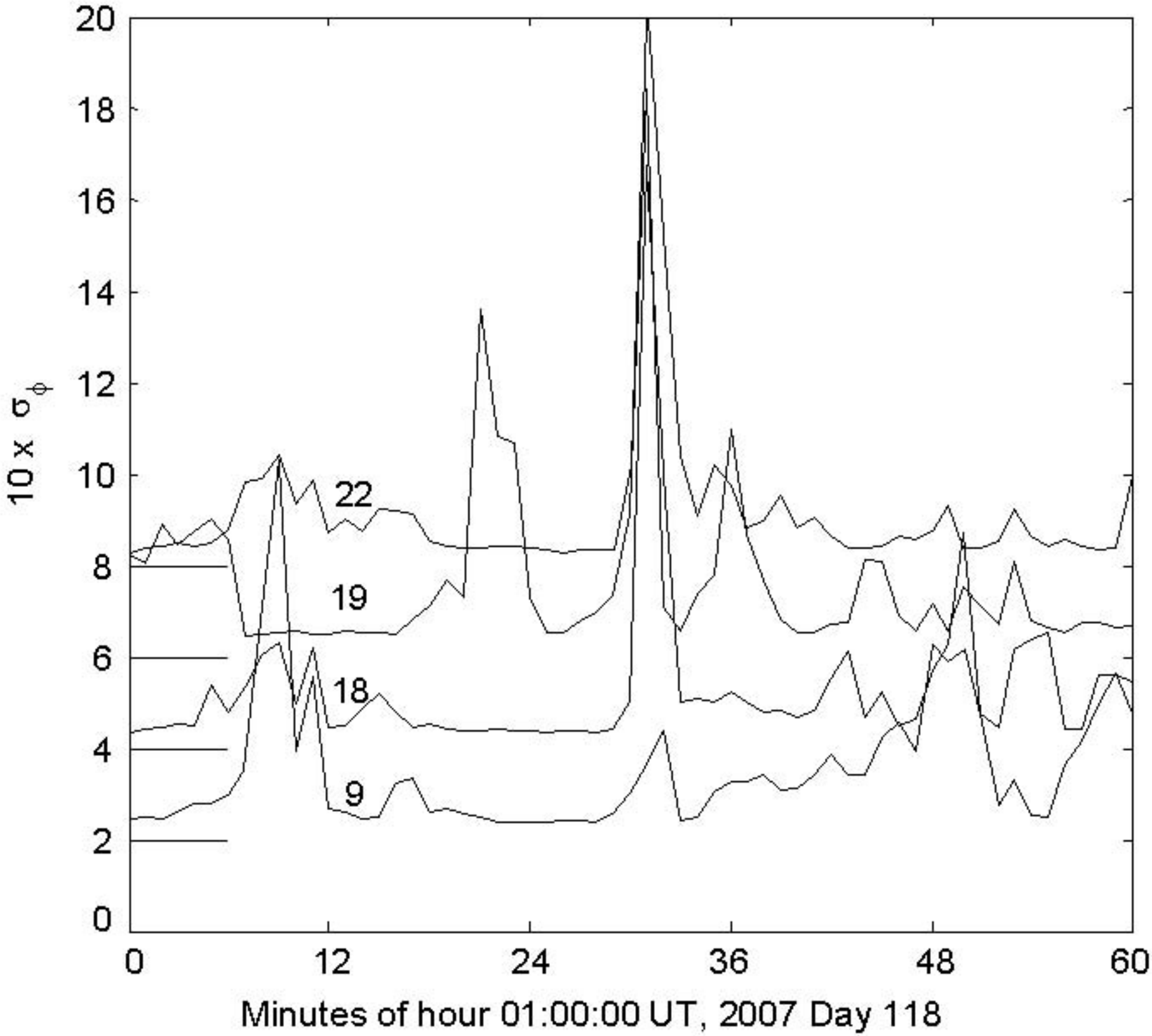
20
18
16
14
12
10
8
6
4
2
0
10 x σφ
22
19
18
9
0
12
24
36
48
60
Minutes of hour 01:00:00 UT, 2007 Day 118

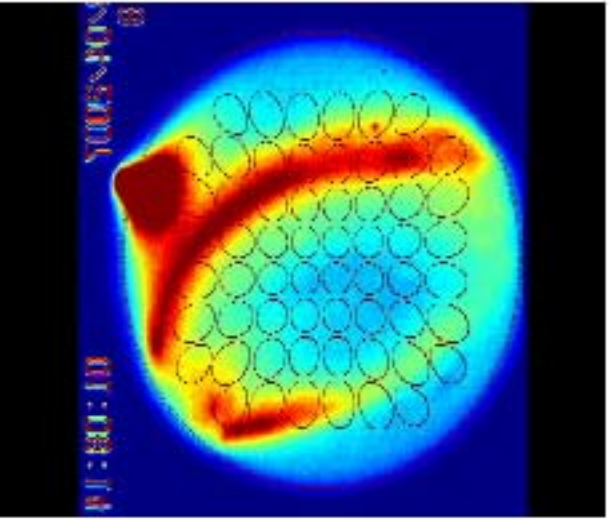

(a) 01:08:14

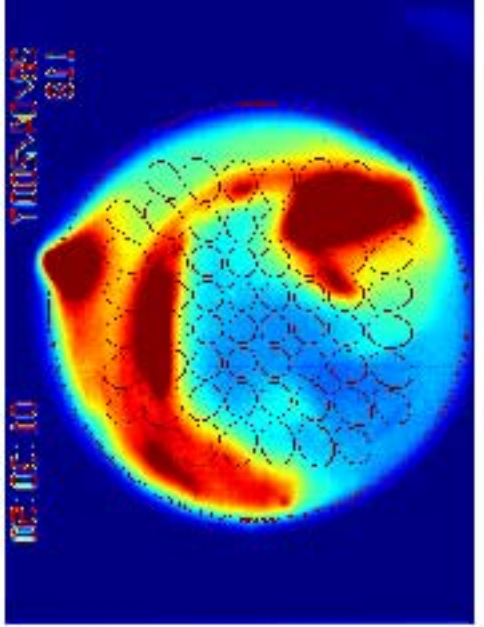

(b) 01:30:50

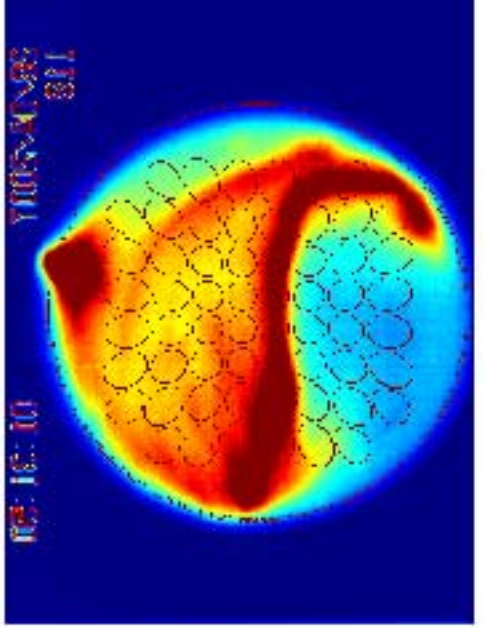

(c) 01:31:50

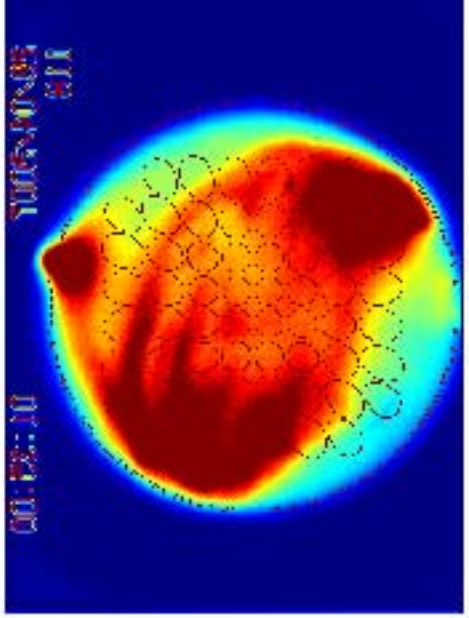

(d) 01:35:00 UT

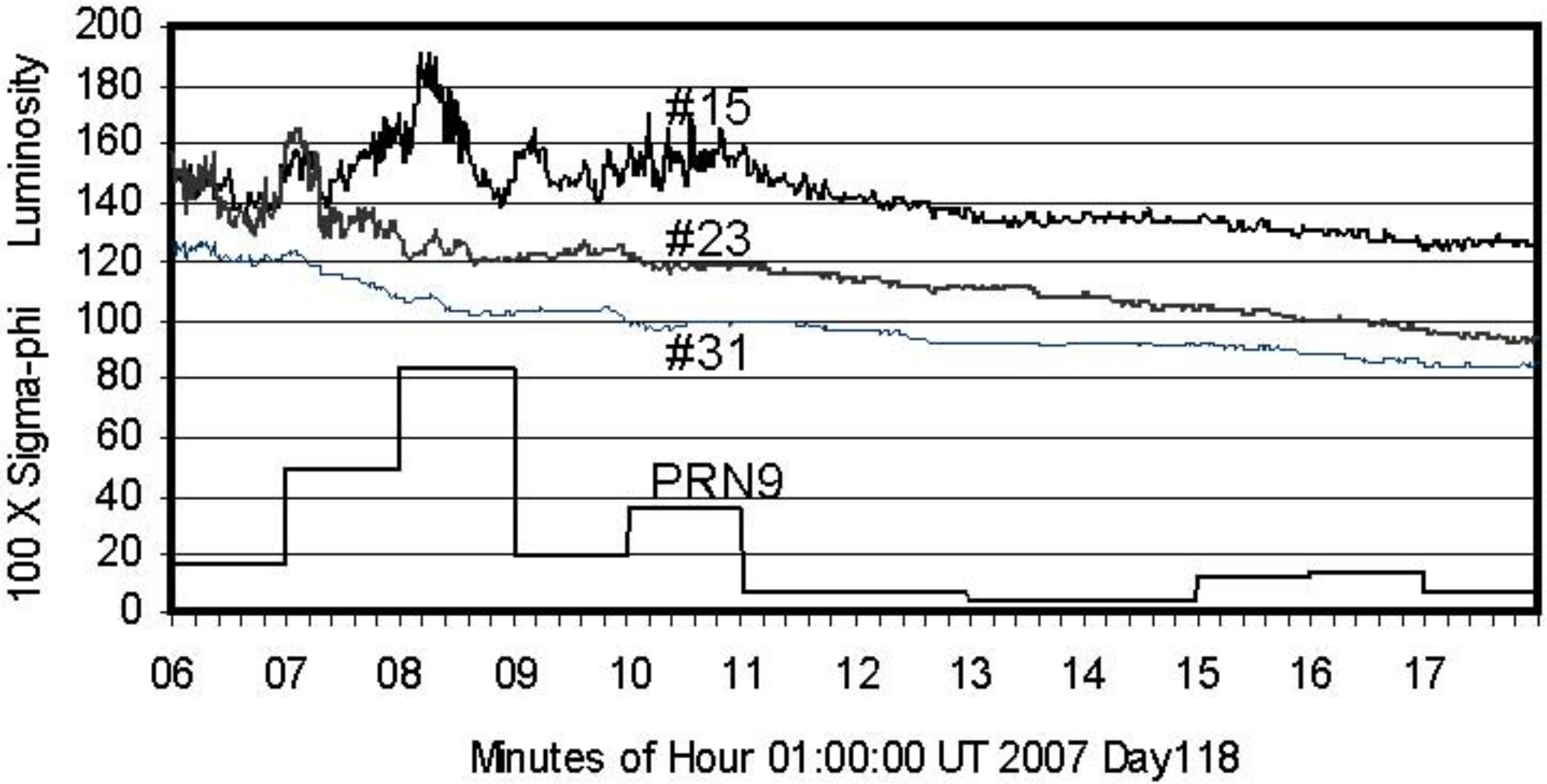
200
180
160
140
120
100
80
60
40
20
0
100 X Sigma-phi Luminosity
#15
#23
#31
PRN9
06
07
08
09
10
11
12
13
14
15
16
17
Minutes of Hour 01:00:00 UT 2007 Day118

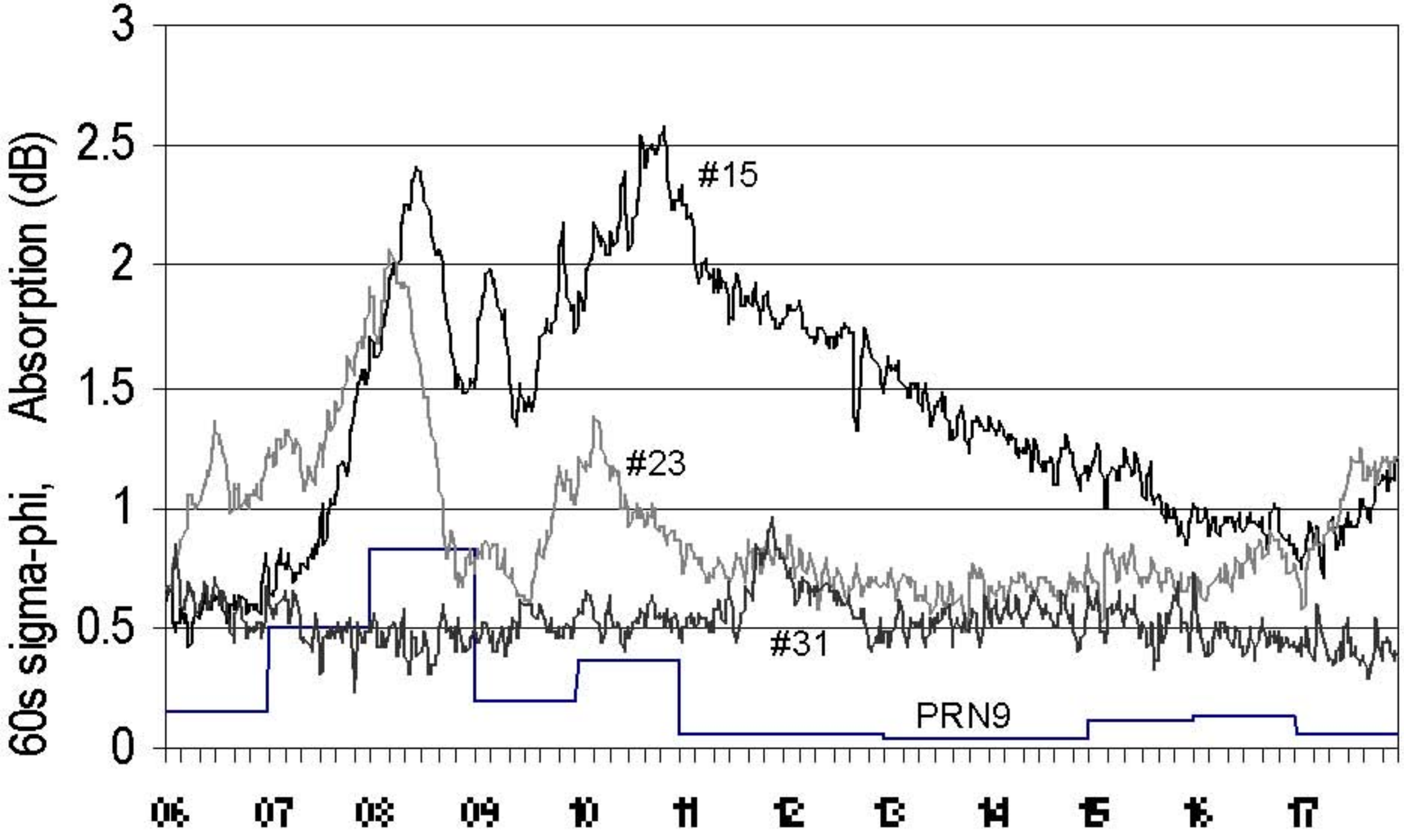
3
2.5
2
1.5
1
0.5
0
Absorption (dB)
60s sigma-phi,
#15
#23
#31
PRN9
06
07
08
09
10
11
12
13
14
15
16
17
Minutes of Hour 01:00:00 UT 2007 Day 118

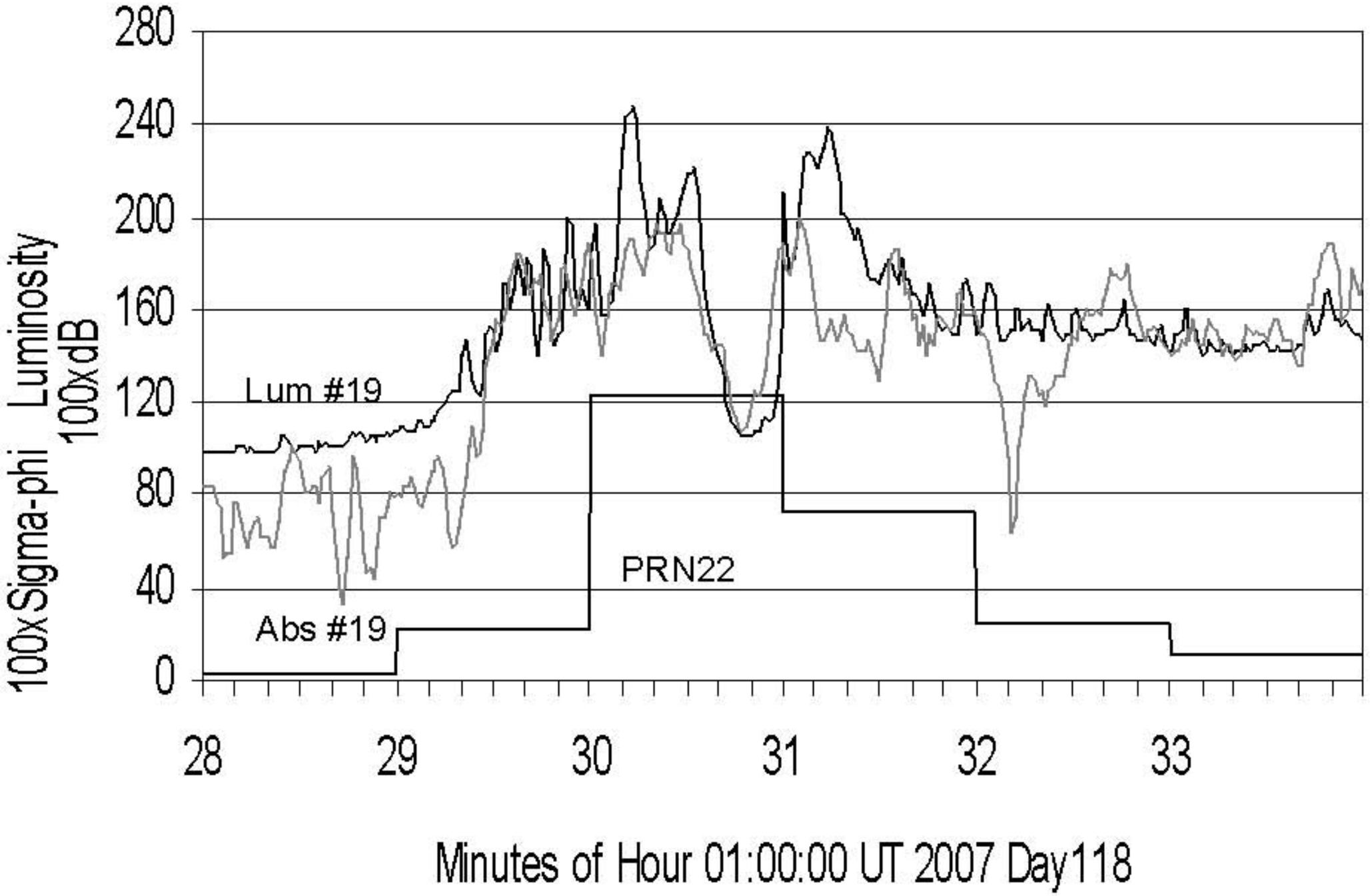
100xSigma-phi Luminosity
100xdB
280
240
200
160
120
80
40
0
Lum #19
PRN22
Abs #19
28
29
30
31
32
33
Minutes of Hour 01:00:00 UT 2007 Day118

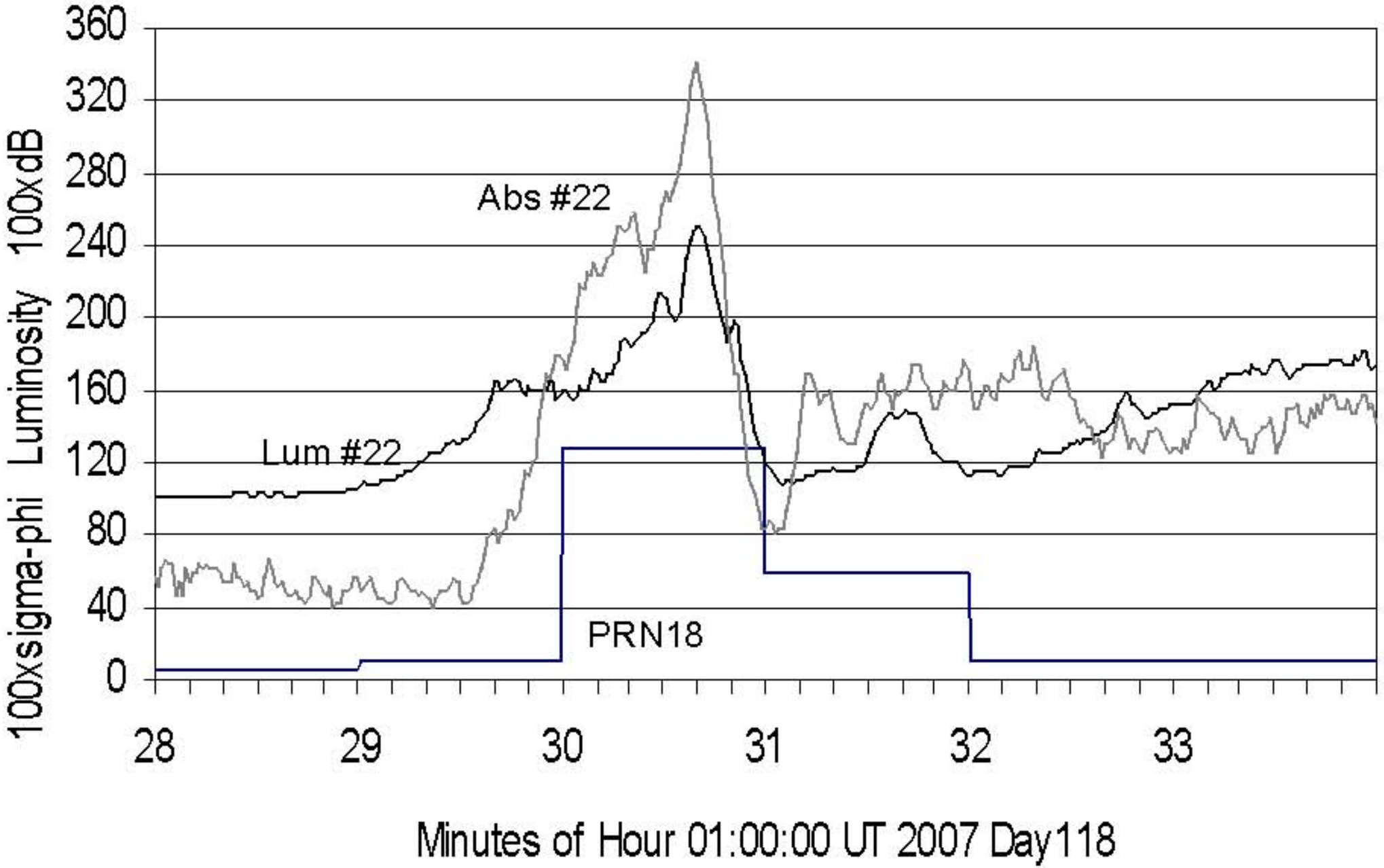
360
320
280
240
200
160
120
80
40
0
100xsigma-phi Luminosity 100xdB
Abs #22
Lum #22
PRN18
28
29
30
31
32
33
Minutes of Hour 01:00:00 UT 2007 Day118

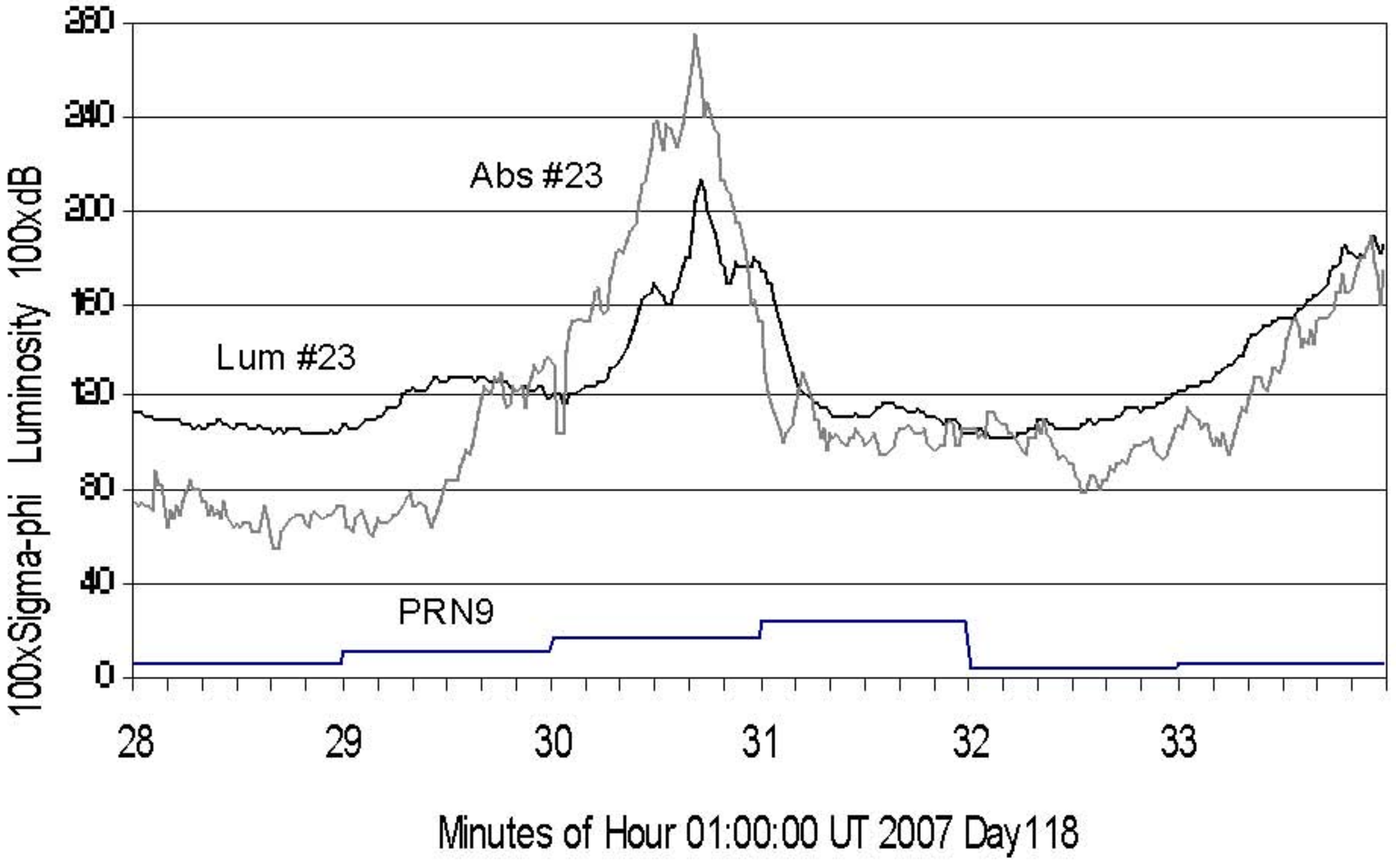
100xSigma-phi Luminosity 100xdB
280
240
200
160
120
80
40
0
Abs #23
Lum #23
PRN9
28
29
30
31
32
33
Minutes of Hour 01:00:00 UT 2007 Day118

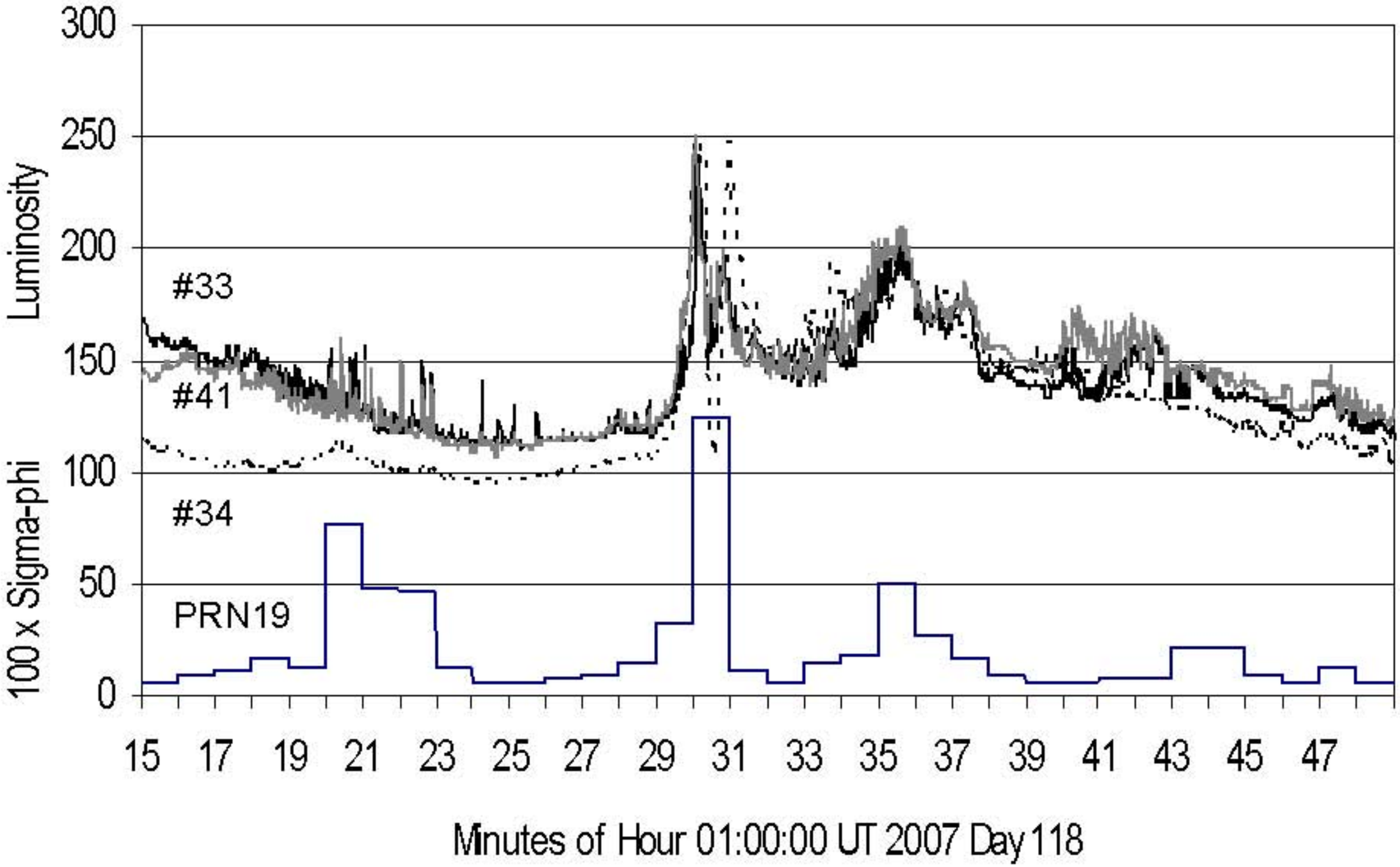
Luminosity
300
250
200
150
100
50
0
#33
#41
#34
PRN19
100 x Sigma-phi
15
17
19
21
23
25
27
29
31
33
35
37
39
41
43
45
47
Minutes of Hour 01:00:00 UT 2007 Day 118

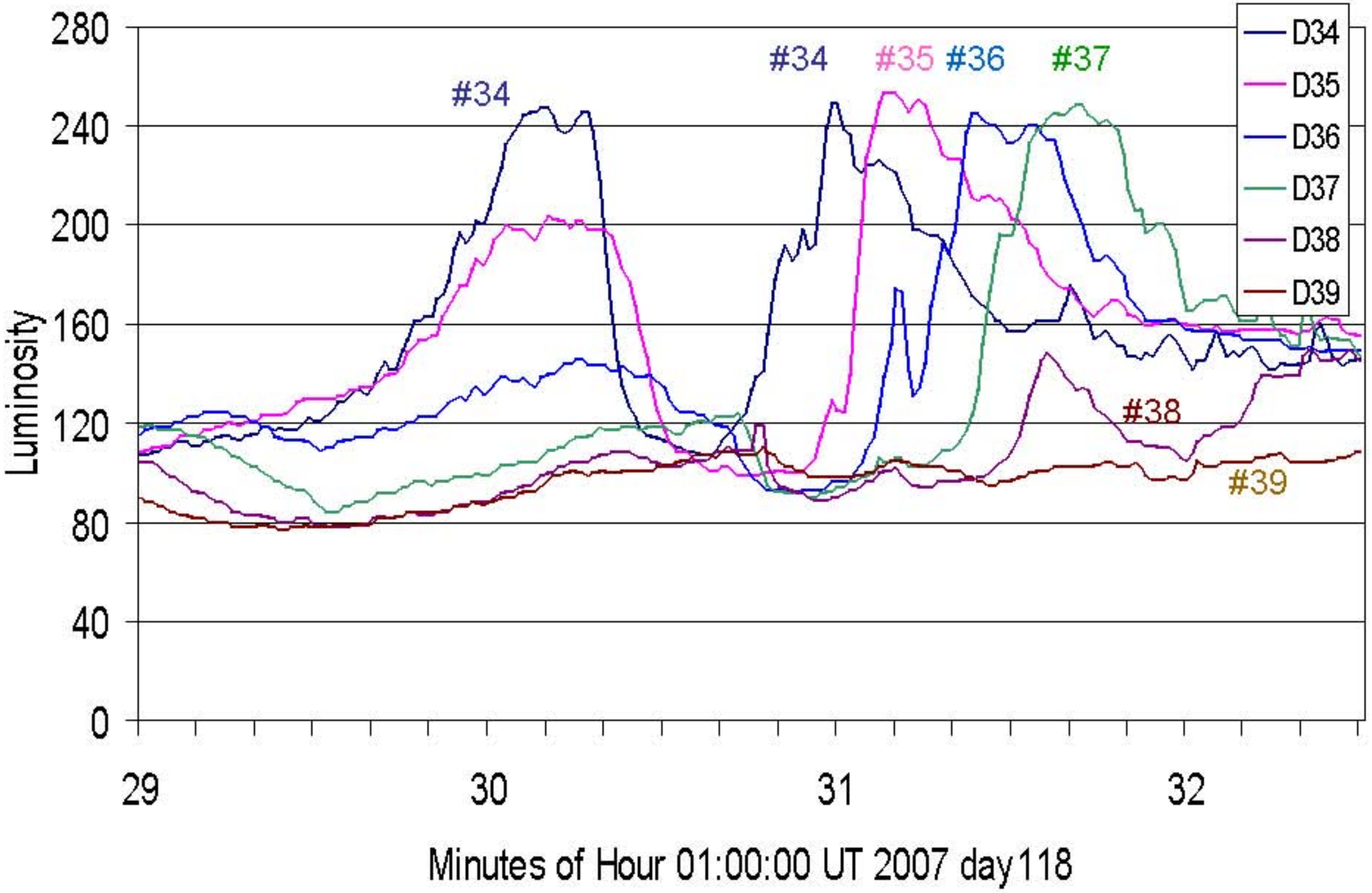
280
240
200
160
120
80
40
0
Luminosity
#34
#34
#35
#36
#37
#38
#39
D34
D35
D36
D37
D38
D39
29
30
31
32
Minutes of Hour 01:00:00 UT 2007 day 118

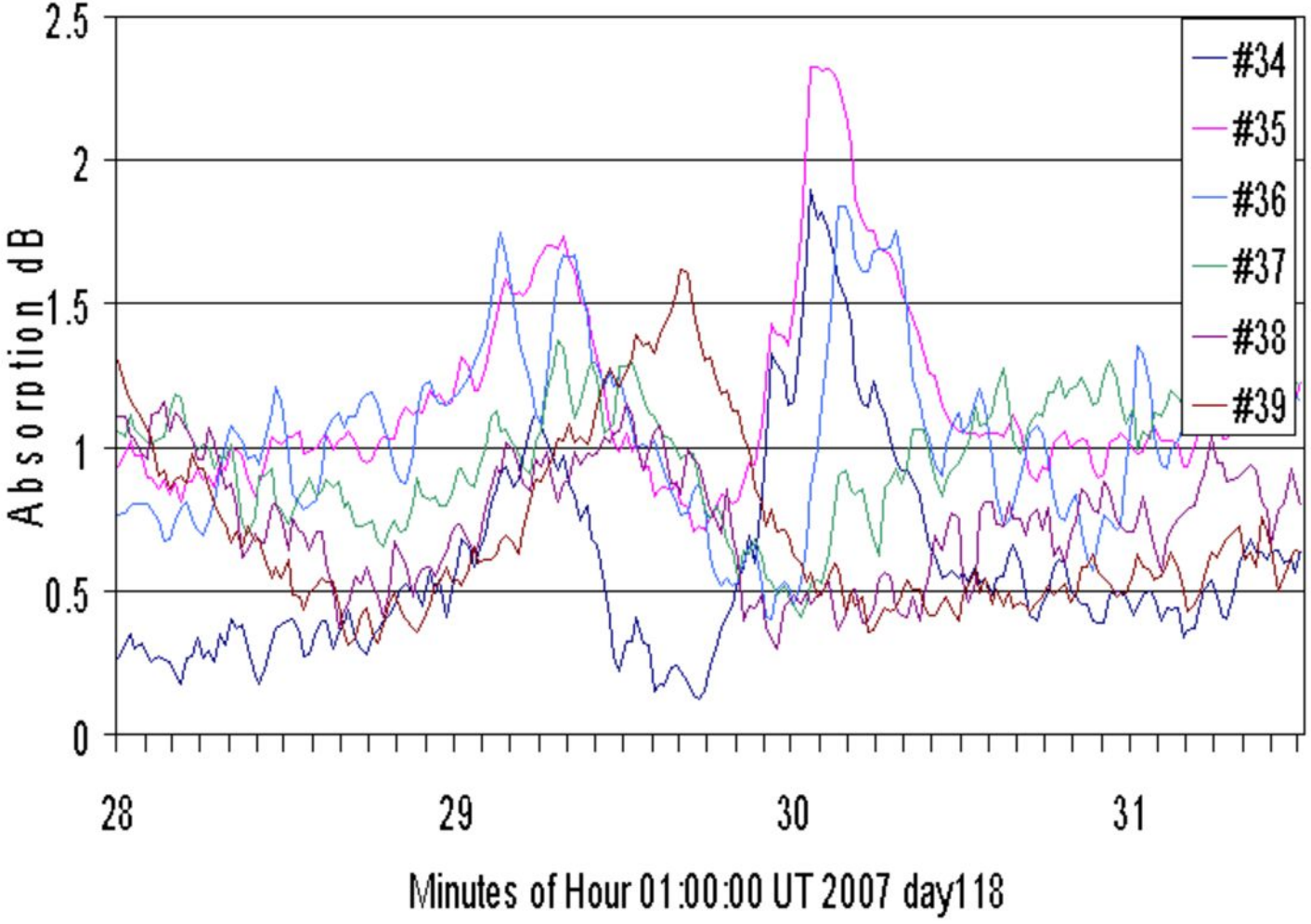
2.5
2
1.5
1
0.5
0
Absorption dB
#34
#35
#36
#37
#38
#39
28
29
30
31
Minutes of Hour 01:00:00 UT 2007 day118

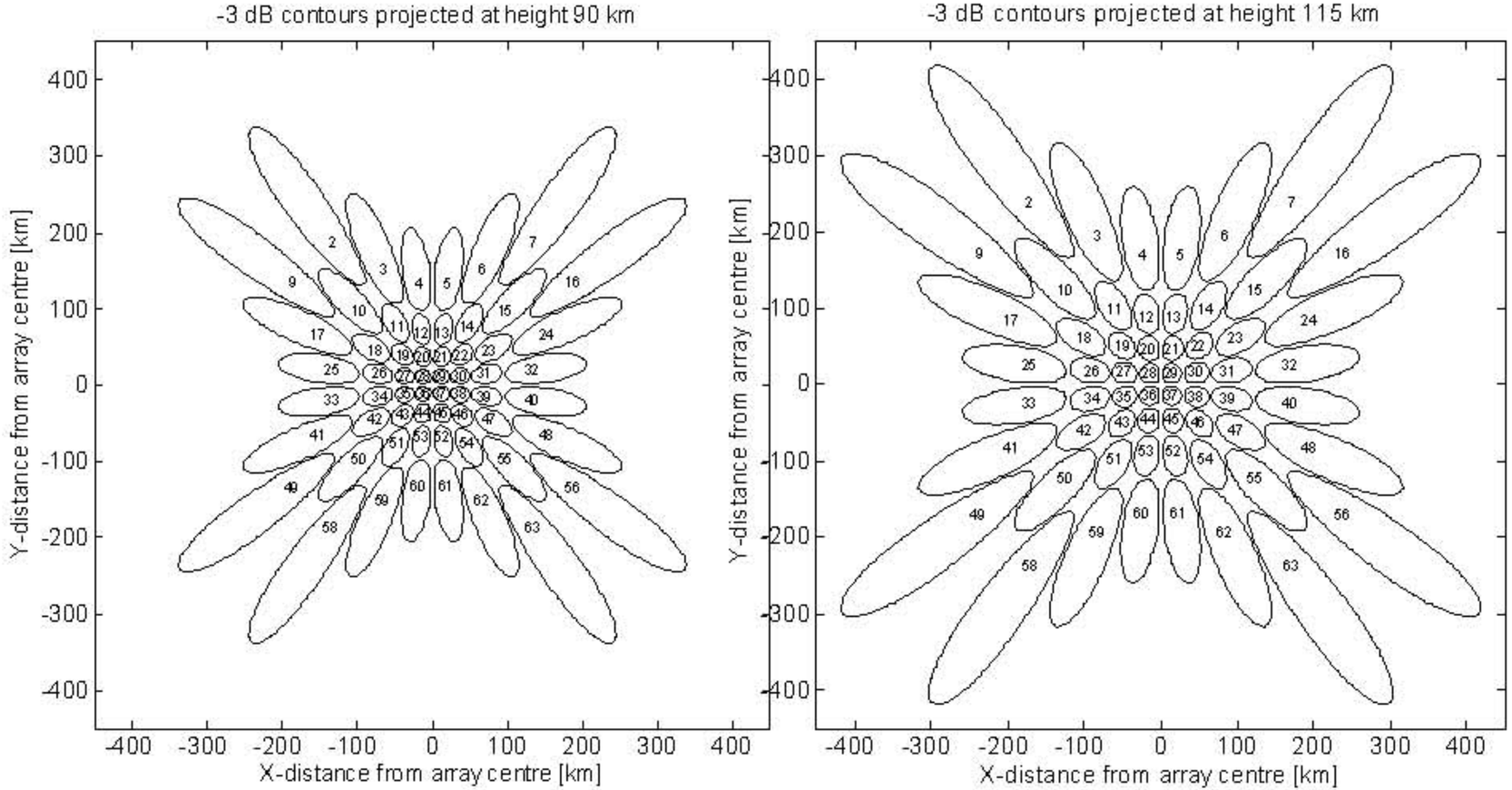
-3 dB contours projected at height 90 km
-3 dB contours projected at height 115 km
Y-distance from array centre [km]
X-distance from array centre [km]
400
300
200
100
0
-100
-200
-300
-400